A magneto-optical study of bismuth-doped $MgO-Al_2O_3-SiO_2$ glass: on the nature of near-infrared luminescence[*]

A.V. Laguta, B.I. Denker, S.E. Sverchkov, I.M. Razdobreev

Abstract. **This paper presents results of a detailed magneto-optical spectroscopy study of bismuth-doped aluminosilicate glass. At least three distinct optical centres are shown to coexist in the glass: bismuth ion clusters, Bi^+ ions and defects in the glass structure, with energy transfer between the last two species. Analysis of magnetic circular dichroism and magnetic circular polarisation of luminescence as functions of magnetic field and temperature indicates that all three centres have an even number of electrons (holes). Experimental evidence is presented that both 'red' and near-infrared luminescence bands are due to transitions in the defects.**

Keywords: *aluminosilicate glass, magnetic circular dichroism, magnetic circular polarisation of luminescence, near-IR luminescence.*

1. Introduction

After the discovery of near-IR (NIR) photoluminescence (PL) in bismuth-doped glass [1, 2], this effect has been the subject of a huge number of experimental and theoretical studies. The increasing interest in bismuth-doped glasses is aroused by their promising potential for practical application in fibre lasers and amplifiers [3]. Such devices are widely used not only in telecommunication systems but also in medical applications, materials processing and scientific research [4]. Despite the significant advances in the development of bismuth-doped fibre lasers [4], there are still a number of unanswered crucial questions and unresolved important issues. First, amplification and lasing can only be obtained at low doping levels. As a consequence, rather long lengths of fibre are needed for efficient operation of devices. Another problem is the considerably lower efficiency of such lasers and amplifiers in comparison with their rare-earth-doped counterparts. Finally, a critical issue is the very poor understanding of the nature of the NIR luminescence, which remains the subject of serious controversy [5].

Since no significant advances in gaining insight into the nature of this PL have been ensured by conventional laser spectroscopy techniques in the past 16 years, we have resorted to more advanced, magneto-optical spectroscopy techniques that take advantage of magnetic circular dichroism (MCD) [6] and magnetic circular polarisation of luminescence (MCPL) [7]. Previously, this approach was successfully used to study sol–gel derived pure SiO_2 glass singly doped with bismuth [8]. In particular, the NIR luminescence in question was shown to be related to even-electron centres.

Both MCD and MCPL are related to the Zeeman effect and provide valuable information about the splitting of the ground state (GS) and excited states (ES's) in a magnetic and a crystal field. In addition, these techniques are relatively easy to implement. For these reasons, the MCD and MCPL techniques are rather widely used in studies of paramagnetic centres. Their only drawback seems to be their relatively low accuracy in determining parameters of a system in comparison with resonance techniques, e.g. electron spin resonance (ESR) and optically detected ESR (ODESR). MCD spectroscopy evaluates the difference between the absorption coefficients for right (σ^+) and left (σ^-) circularly polarised light. In the case of MCPL, one measures the difference between the intensities of the σ^+ and σ^- PL components. In general, the quantitative effect is treated in both cases as the sum of contributions from three terms: A, B and C [9]. The (diamagnetic) A-term arises from degeneracy of the final state of an optical transition and is only dependent on the magnetic field. If there are two closely spaced levels, a magnetic field will mix their wave functions, producing the B-term, which is also temperature-independent. If the initial state is degenerate, there is a (paramagnetic) C-term, which is due to the difference in population between magnetic sublevels, corresponding to a usual Boltzmann distribution, and hence depends not only on the magnetic field but also on temperature. Thus, measuring MCD and MCPL as functions of magnetic field and temperature, we can separately probe the ground and excited states of a transition.

2. Experimental

We studied aluminosilicate glass with the composition $22.2\ \text{mol}\%\ MgO + 22.2\%\ Al_2O_3 + 55.6\%\ SiO_2 + 0.5\%\ Bi_2O_3$, prepared by a standard procedure: melting in a crucible [10]. The melting point of such glass (below $\sim 1500\,°C$) is substantially lower than that of pure silica glass, and its optical characteristics are similar to those of bismuth-doped aluminosilicate fibres fabricated by MCVD. In MCD measurements, we used lock-in detection with a silicon (350 – 900 nm) or germanium (900 – 1800 nm) photodetector. In the longer wavelength range, we were limited by a wavelength of 1550 nm, which was caused by the presence of anti-reflection

---

A.V. Laguta, I.M. Razdobreev CERLA, PHLAM UMR CNRS 8523, University Lille-1, Lille 59655, France;
e-mail: oleksii.laguta@univ-lille1.fr, igor.razdobreev@univ-lille1.fr;
B.I. Denker, S.E. Sverchkov A.M. Prokhorov General Physics Institute, Russian Academy of Sciences, ul. Vavilova 38, 119991 Moscow, Russia;
e-mail: glasser@lst.gpi.ru

coatings on some optical elements. Technical aspects of MCD spectrometers can be found in an excellent review by Denning [11]. A sample was placed in a magneto-optical closed-cycle helium cryostat (SpectromagPT, Oxford Instruments). The system enables measurements in a wide temperature range (1.4–300 K) in magnetic fields up to 7 T. The MCD signal is determined as $\Delta A = A^+ - A^-$, where A^+ and A^- are the absorption coefficients for right and left circularly polarised light. The MCPL signal was measured using a photon counting technique, and the degree of luminescence polarisation was determined as $\Delta_{MCPL} = (I^+ - I^-)/I_{total}$, where I^+ and I^- are the intensities of the σ^+ and σ^- components and $I_{total} = I^+ + I^-$. The MCPL spectrometer used in this study was described in detail previously [8].
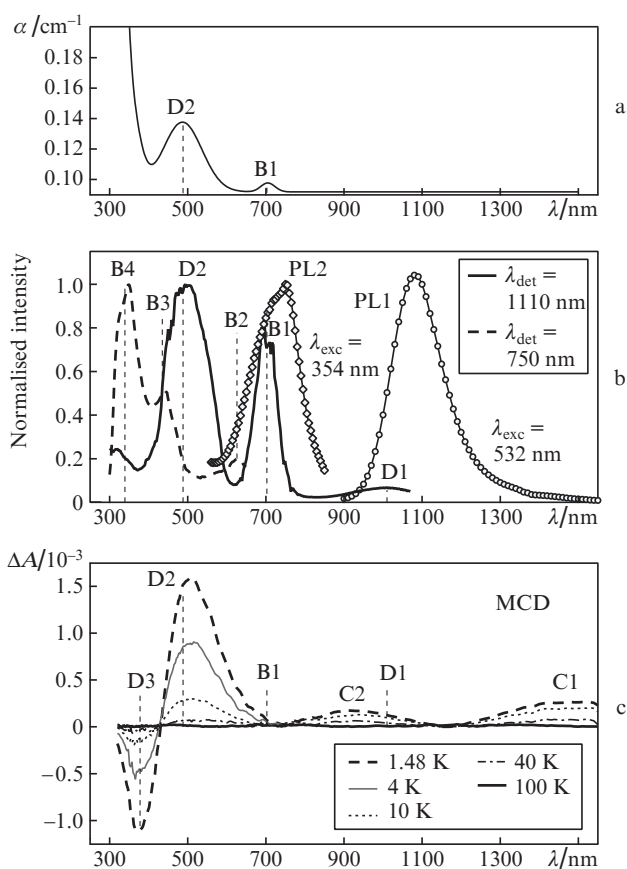
3. Results

3.1. Absorption, excitation, MCD and MCPL spectra

Figures 1a and 1b show room-temperature absorption and excitation spectra of the glass. In the wavelength range 400–1550 nm, only two absorption bands are seen, denoted as D2 and B1, which are centred at 500 and 700 nm, respectively. These bands coincide with two bands in the excitation spectrum of the NIR photoluminescence band PL1 at a detection wavelength $\lambda_{det} = 1110$ nm. The spectrum of the PL1

Figure 1. (a) Absorption spectrum and (b) normalised excitation (——, ---) and PL (o, ◇) spectra at room temperature; (c) MCD spectra at various temperatures in a magnetic field of 6 T. The following notation is used for the peaks: Bi, Bi$^+$; Di, defect; and Ci, bismuth ion clusters (see text).

band is also shown in Fig. 1b. The excitation spectrum allows one to detect an additional, weak feature, D1, in the NIR spectral region, peaking at a wavelength of 1030 nm. Clearly, this feature corresponds to the first excited state of the luminescence centre. Emission from this level is observed as the NIR band PL1, with a Stokes shift of ∼700 cm^{-1}. Since both bands, D2 and B1, are present in the excitation spectrum of the NIR band PL1, it is reasonable to assume that they arise from the same optical centre. At the same time, the excitation spectrum of the luminescence band PL2 at a detection wavelength of 750 nm has three bands, peaking at $\lambda = 625$, 441 and 340 nm, which do not coincide with any of the bands in the excitation spectrum of the NIR band PL1. This contradiction can be accounted for by the existence of two distinct types of centres, with energy transfer between them. In previous work [12], such transfer was demonstrated experimentally for bismuth–gallium (Bi/Ga) codoped silica glass, an analogue of the aluminosilicate glass under consideration. The energy transfer presumably results from quadrupole–quadrupole interaction between the two centres. It is this which accounts for the presence of the B1 band in the excitation spectrum of the NIR luminescence band.

Unlike the absorption spectrum, the MCD spectrum in Fig. 1c has four bands: one negative band, peaking at $\lambda = 375$ nm (D3), and three positive bands, peaking at $\lambda = 505$ (D2), 940 (C2) and 1500 nm (C1). All these bands are temperature-dependent, which unambiguously indicates that the corresponding ground states are spin multiplets. That the absorption and MCD spectra have only one band in common (centred near $\lambda = 500$ nm) is additional strong evidence in support of the assumption that the B1 and D2 bands originate from different optical centres. Clearly, the D2 band is due to a transition from a degenerate ground state. The near-zero MCD signal at wavelengths around $\lambda = 700$ nm, in turn, clearly indicates that the B1 band is due to a centre with a nondegenerate ground state. Thus, the D2 band cannot be assigned to the Bi$^+$ $^3P_0 \rightarrow {}^1D_2$ or $^3P_0 \rightarrow {}^1S_0$ transition, in contrast to what was assumed in many reports, e.g. by Meng et al. [13] and Zhou et al. [14]. On the other hand, the B1 band is attributable to a transition to the $^3P_1$ degenerate level of the Bi$^+$ ion (E state with local symmetry C$_{3v}$). This assumption is quite consistent with our experimental finding that there is no MCD at wavelengths corresponding to the B1 band, i.e. near $\lambda = 700$ nm, because the ground state $^3P_0$ of the Bi$^+$ ion is nondegenerate. It is worth noting that the degeneracy of the final state of this transition may cause an A-term to appear in the expression for the magnitude of the MCD effect. Nevertheless, at low temperatures the A-term for broad bands, which is the case with the samples under study, is three orders of magnitude smaller than the C-term [15]. Based on this hypothesis, we believe that the other bands in the B series, namely the B2, B3 and B4 bands, correspond to the $^3P_0 \rightarrow {}^3P_2$ ($M_J = 0$), $^3P_0 \rightarrow {}^3P_2$ ($M_J = \pm 1$) and $^3P_0 \rightarrow {}^1D_2$ ($M_J = 0$) transitions, respectively. The temperature dependences of the MCD bands in the C and D series differ markedly, so we assume that they have different origins as well.

Figure 2 shows PL (I_{total}) and MCPL ($I^+ - I^-$) spectra in the NIR spectral region under excitation in the D2 absorption band ($\lambda_{exc} = 532$ nm). The MCPL spectrum is temperature-dependent and, hence, the initial state of the radiative transition is a spin multiplet. The MCPL spectrum is shifted to longer wavelengths by 250 cm^{-1} with respect to the luminescence band, and the MCPL peak with $\Delta_{MCPL} = -0.024$, obtained at
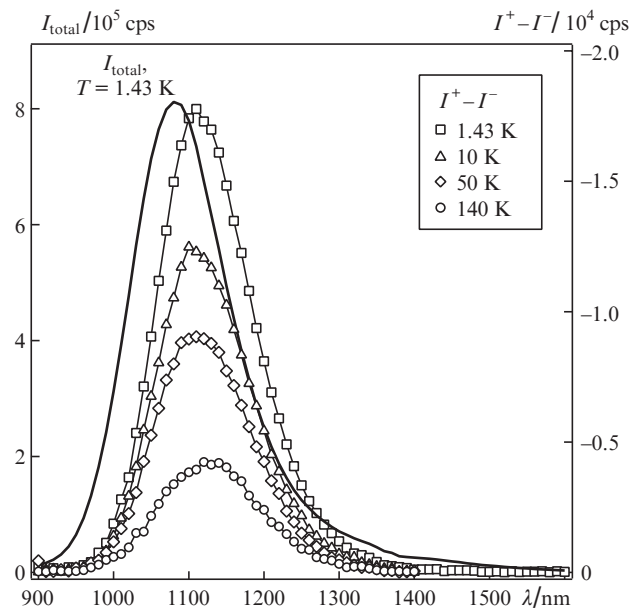
**Figure 2.** Infrared PL and MCPL spectra at various temperatures in a magnetic field of 6 T under excitation in the D2 band ($\lambda_{exc} = 532$ nm).

a temperature of 1.43 K in a magnetic field $B = 6.0$ T, is located at $\lambda = 1110$ nm. One possible cause of the shift is that the luminescence band comprises a short-wavelength wing, determined primarily by a transition from an $M_S = 0$ excited state sublevel, and a long-wavelength part, determined predominantly by emission from an $M_S \neq 0$ sublevel.

In the visible range, excitation at $\lambda = 532$ nm produces a broad emission band centred at $\lambda = 700$ nm (Fig. 3). The MCPL signal is a strong function of temperature. At low temperatures, the signal is negative and peaks at a wavelength of 660 nm. With increasing temperature, the MCPL changes its sign. At $T = 17$ K, the peak is located at $\lambda = 690$ nm. The change in MCPL sign can only be accounted for under the assumption that the luminescence is contributed by at least two different transitions. The transitions may in principle occur in either one optical centre or different centres.
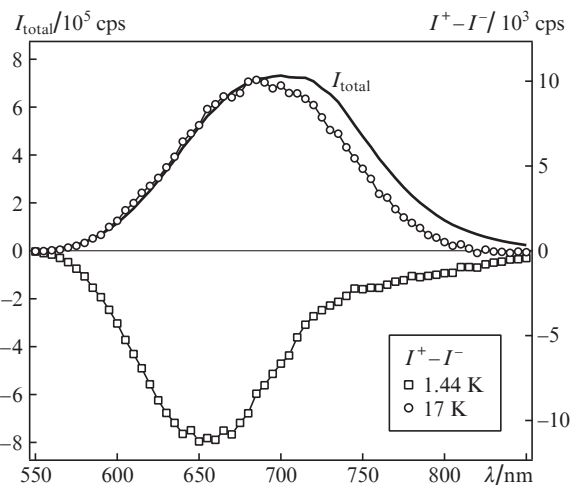
Figure 3. PL and MCPL spectra in a magnetic field of 6 T; $\lambda_{exc} = 532$ nm.

Under excitation at $\lambda_{exc} = 354$ nm (B4 band), the 'red' luminescence is slightly shifted to longer wavelengths, so that the peak emission wavelength is $\lambda = 750$ nm, as shown in Fig. 4. Clearly, like under pumping at $\lambda = 532$ nm, this band consists of several components, as evidenced by MCPL measurements. In addition to the MCPL band centred at $\lambda = 700$ nm, there is a weak feature peaking at $\lambda = 800$ nm. It is seen from the temperature variation of the spectra that, with increasing temperature, the polarisation of this feature decreases considerably more slowly than that of the 700-nm band. The other luminescence band is centred at 460 nm, but its polarisation is strongly shifted to shorter wavelengths. The corresponding MCPL band is also temperature-dependent and essentially disappears at $T = 17$ K.
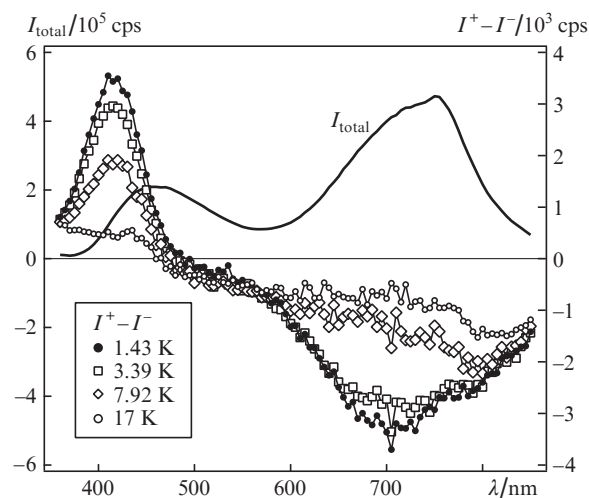

Figure 4. PL and MCPL spectra at various temperatures in a magnetic field of 6 T; $\lambda_{exc} = 354$ nm.

3.2. Field and temperature dependences

MCD saturation curves were obtained for the peaks of the C2 and D3 bands. The C1 and D2 bands were studied previously [16]. Figure 5a shows the field dependences of MCD at $\lambda = 375$ nm. The saturation curves obtained by plotting ΔA against $\mu_B B/(2kT)$ are essentially identical and have a tendency to saturate in strong fields. Temperature dependences were obtained in various magnetic fields, and the data are presented in Fig. 5b as plots of the MCD signal against inverse temperature. The curves also have no anomalies. The MCD signal rises monotonically with decreasing temperature. It is worth noting that the present results are essentially identical to those obtained previously for the D2 band, so it is quite reasonable to think that the D2 and D3 bands are due to the same centre. At first glance, this centre should have an odd number of electrons (or holes), because the shape of the temperature dependences is characteristic of a Kramers doublet [17]. Nevertheless, fitting these curves revealed zero-field splitting of the levels, which is possible only in the case of a non-Kramers doublet, i.e. in an integer-spin system.

In the NIR region, increasing the magnetic field leads to well-defined saturation (Fig. 5c), which clearly points to a high g-factor, whereas divergence of isotherms means that the ground state is a non-Kramers doublet [17]. In magnetic fields of 3 T and above, the temperature dependences shown in Fig. 5d saturate at a temperature of 5 K or below and are very
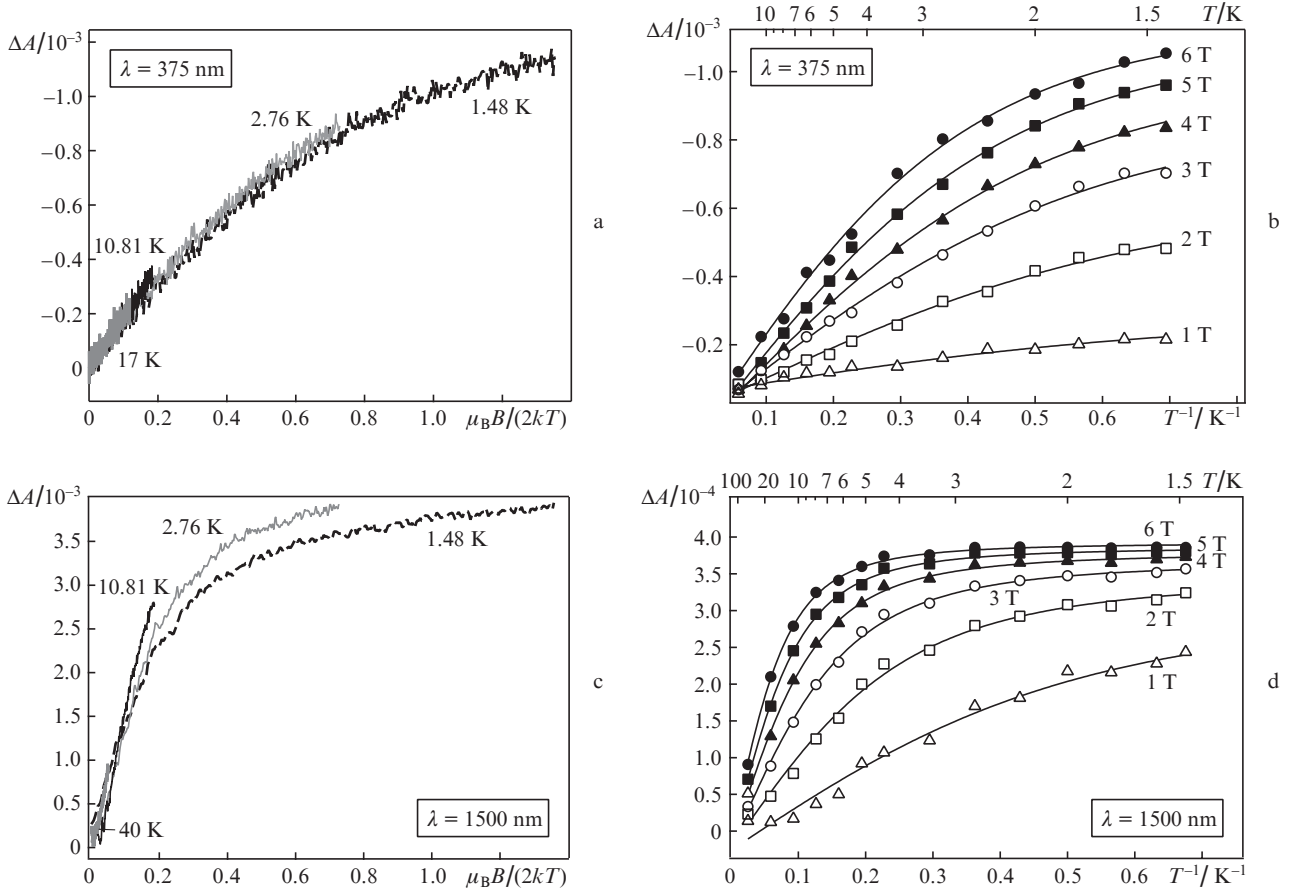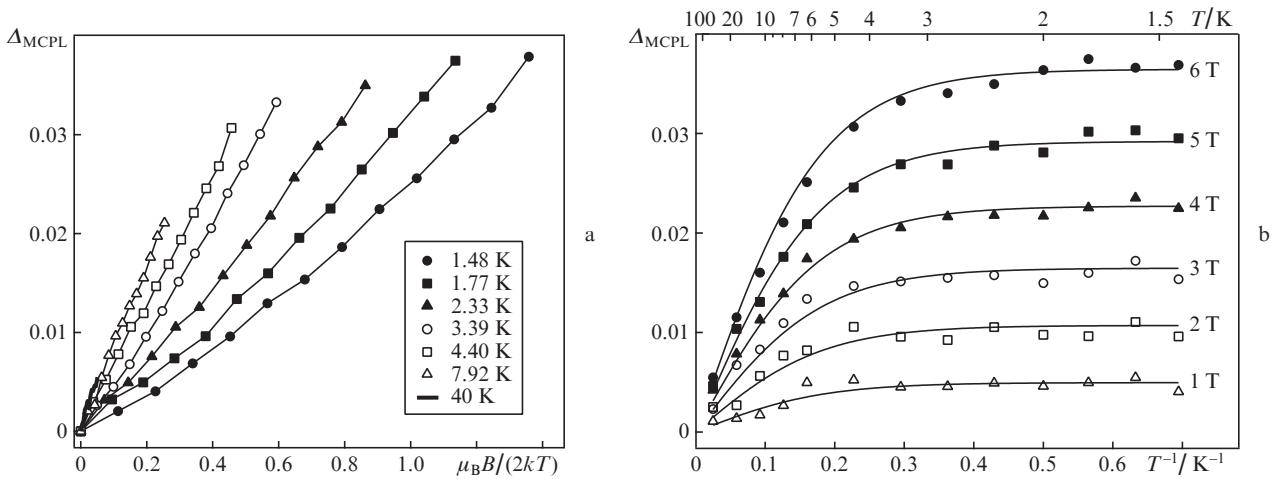
Figure 5. MCD signal ΔA (a, c) as a function of magnetic field at various temperatures and (b, d) as a function of temperature in constant fields. The solid lines in Figs 5b and 5d represent theoretical curves obtained using relation (2a) at $N = 1$.

closely spaced. Such behaviour is characteristic of even-electron systems.

Figure 6 presents MCPL saturation curves obtained at $\lambda =$ 415 nm under excitation at $\lambda =$ 354 nm. The field dependences show a high degree of divergence and there is no saturation even in high magnetic fields or at low temperatures. Note that, if the degree of MCPL is represented as a function of

$1/T$, to each magnetic field there corresponds a certain Δ_{MCPL} value at saturation (Fig. 6b). This behaviour of the MCPL signal can be accounted for by a low g-factor and large zero-field splitting.

The effects of magnetic field and temperature on the MCPL was also studied in detail for the red luminescence band at detection wavelengths of 660 and 700 nm, which cor-

**Figure 6.** MCPL signal Δ_{MCPL} (a) as a function of magnetic field at various temperatures and (b) as a function of temperature in constant fields: $\lambda_{exc} =$ 354 nm, $\lambda_{det} =$ 415 nm. The solid lines in Fig. 6b represent theoretical curves obtained using relation (2b) at $N = 1$.

respond to the position of the MCPL peaks under excitation at wavelengths of 532 and 354 nm, respectively. The temperature dependences obtained at λ_{det} = 660 nm are presented in Fig. 7a. It is seen that the curves have a rather nontrivial shape. With decreasing temperature, the MCPL signal increases, reaching the maximum value Δ_{MCPL} = 0.016 at T = 17 K in a magnetic field of 6 T. At lower temperatures, Δ_{MCPL} decreases and changes sign at $T \sim 6$ K. As pointed out above, the change in MCPL sign and such nontrivial behaviour of the MCPL can readily be accounted for under the assumption that the luminescence in this region is contributed by different optical transitions. The splitting energies of excited-state spin levels should then differ significantly. At first glance, the temperature dependences obtained at a wavelength of 700 nm (Fig. 7b) exhibit usual monotonic behaviour. However, modelling of the experimental data indicates again that there are two components of opposite sign, like under excitation at a wavelength of 532 nm.

Saturation curves were analysed using a spin Hamiltonian with an axial (D) and a rhombic (E) splitting component [18]:

$$H = D\left[S_z^2 - \frac{1}{3}S(S+1)\right] + E(S_x^2 - S_y^2) + g_{\|}\mu_B B\cos\theta, \quad (1)$$
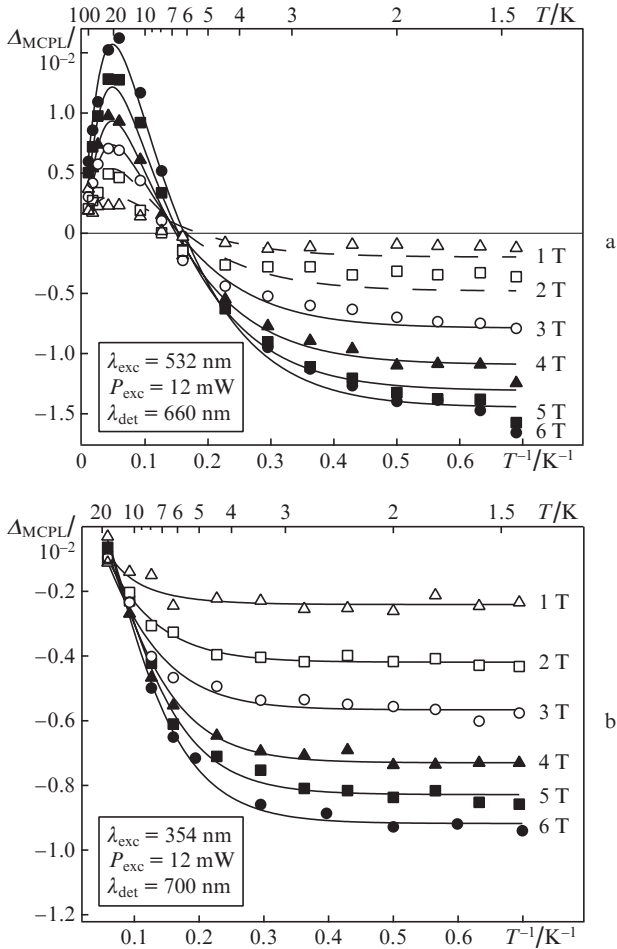
where $g_{\|} = g_{zz} \gg g_{\perp} = g_{xx} = g_{yy}$; μ_B is the Bohr magneton; and θ is the angle between the direction of the external magnetic field B and the z axis. A temperature-dependent C-term may appear only if the initial state is a spin multiplet. In the case of an integer effective spin, e. g. $S = 1$, this is only possible if the axial splitting parameter is negative: $D < 0$. The $M_S = \pm 1$ multiplet will then have the lowest energy, and the rhombic distortion term will completely lift the degeneracy even in the absence of an external magnetic field. In such a case, the wave functions of the $M_S = \pm 1$ states have the form $|\pm\rangle = 1/\sqrt{2}\,(|+1\rangle \pm |-1\rangle)$, the angular momentum is quenched, and, as a consequence, there is no MCD or MCPL effect. A magnetic field, in turn, mixes these states so that the contributions of the $|\pm 1\rangle$ functions become unequal and produces an additional splitting of the levels. The wave functions then become complex-valued:

$$|+\rangle = \cos\alpha\,|+1\rangle + \sin\alpha\,|-1\rangle,$$

$$|-\rangle = \sin\alpha\,|+1\rangle - \cos\alpha\,|-1\rangle,$$

where $\tan(2\alpha) = \Delta/(2g_{\|}\mu_B B\cos\theta)$ and $\Delta = 6|E|$ (Δ is the zero-field splitting energy). Thus, a magnetic field 'unfreezes' the angular momentum, thus causing MCD and MCPL effects. MCD and MCPL saturation curves were fitted with the following expressions [17]:

$$\Delta A = \sum_{i=1}^{N} A_i^{sat} \int_0^1 \frac{2\tilde{g}_i\mu_B B\cos^2\theta}{\sqrt{\Delta_i^2 + (2\tilde{g}_i\mu_B B\cos\theta)^2}}$$

$$\times \tanh\left[\frac{\sqrt{\Delta_i^2 + (2\tilde{g}_i\mu_B B\cos\theta)^2}}{2kT}\right]d\cos\theta, \quad (2a)$$

$$\Delta_{MCPL} = \sum_{i=1}^{N} A_i^{sat} \int_0^1 \frac{2\tilde{g}_i\mu_B B\cos^4\theta}{\sqrt{\Delta_i^2 + (2\tilde{g}_i\mu_B B\cos\theta)^2}}$$

$$\times \tanh\left[\frac{\sqrt{\Delta_i^2 + (2\tilde{g}_i\mu_B B\cos\theta)^2}}{2kT}\right]d\cos\theta. \quad (2b)$$

The summation is carried out over all transitions from different doublets that contribute at a given wavelength, and $\tilde{g}$ is an effective g-factor, which is $4g_{\|}$ at $S = 2$ and $2g_{\|}$ at $S = 1$. Expressions (2a) and (2b) differ only by the factor $\cos^2\theta$, which appears when photoselection is taken into account [19]. The fitting results are summarised in Table 1.

The fitting results for the saturation curves of the MCD signal in the D3 and C2 bands are very similar to those obtained previously for the D2 and C1 bands, respectively. Because of this, they were analysed pairwise. Attention should be paid to the fact that the fitting parameters, namely the zero-field splitting energy Δ and g-factor, for the MCD bands in the D and C series differ significantly. This proves that the Di and Ci bands observed in the MCD spectra are indeed due to different centres and that both centres are even-electron systems. We believe that the Ci bands are attributable to bismuth ion clusters because of their high effective g-factor. In the clusters, there may be spin–spin and/or exchange interaction between the bismuth ions. As a result, the total effective spin of the system differs from the total angular momentum of an individual ion [18]. For example, the effective spin of Mn$_5$ manganese ion clusters is 25/2 [20]. Therefore, the true

Figure 7. Temperature dependences of the MCPL signal Δ_{MCPL} in constant fields at detection wavelengths of (a) 660 and (b) 700 nm. The solid lines in Fig. 6b represent theoretical curves obtained using relation (2b) at $N = 2$.

Table 1. Numerical analysis results; the Sign column specifies the sign of the corresponding MCD/MCPL component.

Method	λ/nm	Sign	$g_\parallel$ $S = 1$	$g_\parallel$ $S = 2$	Δ/cm^{-1}
MCD (GS)	375 (D3), 505 (D2)	–, +	0.9±0.03	0.45±0.02	1.36±0.13
	940 (C2), 1500 (C1)	+, +	4.4±0.02	2.2±0.01	2.77±0.02
MCPL (ES)	415 (λ_{exc} = 354 nm)	+	0.16±0.85	0.08±0.043	7.43±0.37
	700 (PL2, λ_{exc} = 354 nm)	–	0.9±0.25	0.45±0.13	10.8±3
		+	0.35±2	0.18±1	27±7
	660 (λ_{exc} = 352 nm)	–	0.2±0.5	0.1±0.3	7.13±1
		+	0.5±3.7	0.25±1.85	36.3±3.45
	1110 (PL1, λ_{exc} = 352 nm)	–	0.9±1.2	0.45±0.6	43.3±1.4

g-factor can only be found if the effective spin is known. However, it is practically impossible to gain such information by the MCD and MCPL techniques. In view of this, we present *g*-factors for different *S* values in Table 1. It is seen that reasonable values can only be obtained for $S \geqslant 2$, which suggests the presence of clusters. As pointed out above, the field and temperature dependences for the D*i* MCD bands have a shape characteristic of a Kramers doublet. To clarify this issue, we compared the saturation curve fitting results obtained for the D2 band with a Kramers ($\Delta = 0$) and a non-Kramers ($\Delta \neq 0$) doublet. The results are very similar, which is not surprising because of the rather low Δ value predicted by the non-Kramers doublet model. Nevertheless, the χ^2 value (a measure of how well a model describes experimental data) is lower in the case of the non-Kramers doublet. As a result of zero-field splitting, the ESR signal cannot be detected by most widespread spectrometers, which operate in the X-band range because the microwave photon energy is too low: the frequency 9.8 GHz corresponds to an energy of 0.33 cm^{-1}.

Analysis of MCPL saturation curves indicates that the observed bands are due to even-electron centres. It is well known that parameters of a model can be accurately determined only if they make comparable contributions. In the case of a non-Kramers doublet, the energy separation between its sublevels is determined by two factors: Zeeman interaction and crystal field splitting. In the systems under investigation, even in strong magnetic fields it is the crystal field that makes a major contribution to the splitting in excited states. For example, in the first excited state, which is responsible for the NIR luminescence, the splitting energy comprises the crystal field splitting energy $\Delta = 43.3$ cm^{-1} and the Zeeman energy $\tilde{g}\mu_B B = 5$ cm^{-1} at $B = 6$ T. It is seen that the latter contribution is much smaller, by almost one order of magnitude, so the error of determination of the *g*-factor is large. On the other hand, in the ground state these energies are comparable and, as a consequence, both can be determined with high accuracy.

Under excitation at a wavelength of 532 nm, the MCPL in the red luminescence band consists of two components of opposite sign. The negative, shorter wavelength component has a lower crystal field splitting energy. It is for this reason that, measuring the MCPL spectrum at various temperatures, we were able to accurately separate these components. At low temperatures, the negative component prevails. With increasing temperature, it decreases, whereas the positive component still has a relatively high degree of polarisation because of the higher zero-field splitting energy. As a result, the temperature dependence of the MCPL has a nontrivial shape, with a maximum near 17 K. As pointed out above, two negative bands can be identified in the MCPL spectrum in the range

550–850 nm under excitation at a wavelength of 354 nm. Since the longer wavelength band, which is most likely due to the Bi$^+$ ion, has an essentially zero intensity near 700 nm, it is reasonable to assume that the MCPL at this wavelength has only one, negative component. However, satisfactory fitting results for the temperature dependences in Fig. 7b (λ_{det} = 700 nm) were only obtained when the model included two spectral components with opposite MCPL signs. Most likely, we deal here with the same MCPL bands as under excitation at a wavelength of 532 nm. The red luminescence in bismuth-doped glasses and crystals is commonly attributed to the $^2P_{3/2} \rightarrow {}^2P_{1/2}$ transition of the Bi^{2+} ion [14, 21–23], but our experimental data provide conclusive evidence that the bismuth-doped aluminosilicate glass contains no odd-electron systems, i.e. no Bi^{2+} ions. It is well known that silica glass may contain nonbridging oxygen hole centres, which have a luminescence band centred near 650 nm [24]. However, this centre also has an odd number of electrons, so it cannot be responsible for the red luminescence. Below, we clarify the origin of this luminescence. It is worth noting that analysis of the present results is complicated by the fact that pumping at $\lambda = 354$ nm leads to a concurrent excitation of both the Bi$^+$ ion and the centre responsible for the D*i* bands.

3.3. Detection of MCD via luminescence

Experimental studies of MCD and MCPL provide no direct information about the degeneracy of multiplets. Analysis of optical transitions in a defect in an external magnetic field indicates that the effective spin of the ground and excited states can be both 1 and 2. To clarify this issue, we performed an additional experiment aimed at detecting MCD in luminescence. On the whole, the idea of the experiment is to assess the influence of MCD on the NIR luminescence intensity. Because of the MCD effect, the total luminescence intensity at low temperatures in strong magnetic fields may depend on whether the luminescence is excited by σ^+- or σ^--polarised light. To make an order-of-magnitude estimate of the effect, we introduce the dimensionless parameter

$$\Delta I_{PL} = (I_{total}(\sigma_p^+) - I_{total}(\sigma_p^-))/(I_{total}(\sigma_p^+) + I_{total}(\sigma_p^-)), \quad (3)$$

where $I_{total}(\sigma_p^+)$ and $I_{total}(\sigma_p^-)$ are the total luminescence intensities under excitation by σ_p^+- and σ_p^--polarised light, respectively. In the simplest model depicted in Fig. 8a, in accordance with selection rules the first excited state is populated through the $^g|1,+1\rangle \rightarrow {}^e|1,0\rangle$ and $^g|1,-1\rangle \rightarrow {}^e|1,0\rangle$ channels, where the subscripts g and e denote the ground and excited states,

Figure 8. Diagrams of energy levels and transitions illustrating MCD detection in NIR PL: (a) the ground and excited states are triplets; (b) the ground state is a triplet and the excited state is a quintet. The solid arrows represent optical transitions and the dashed arrows represent spin–lattice relaxation.

respectively. As a result of spin–lattice relaxation processes, the luminescence will be contributed by the $^{e}|1,0\rangle \to {}^{g}|1,\pm1\rangle$ and $^{e}|1,\pm1\rangle \to {}^{g}|1,0\rangle$ transitions. Owing to the Boltzmann distribution of the population of the magnetic sublevels of the ground state, absorption from the $^{g}|1,+1\rangle$ magnetic sublevel (σ^{+} component) is stronger than that from the $^{g}|1,-1\rangle$ sublevel (σ^{-} component). Clearly, this distinction will lead to a change in total luminescence intensity in response to a change in pump polarisation. Identical reasoning is valid if the ground state is a quintet ($S = 2$) and the effective spin of the

excited state is 1 or 2, because the excited-state level can also be pumped through only two channels. It is worth noting that the effect should be rather strong for these three schemes. Analysis of rate equations suggests that the expected magnitude of the effect is $\sim 10^{-2}$.

A different situation arises in the case of the scheme depicted in Fig. 8b. Here, the excited-state level can be populated through four channels: $^{g}|1,+1\rangle \to {}^{e}|2,0\rangle$, $^{g}|1,-1\rangle \to {}^{e}|2,0\rangle$, $^{g}|1,-1\rangle \to {}^{e}|2,-2\rangle$ and $^{g}|1,+1\rangle \to {}^{e}|2,+2\rangle$. Clearly, in this case, too, optical pumping will cause spin polarisation in the excited state. Nevertheless, this will have no effect on the total luminescence intensity. As in the case of a triplet excited state, absorption from the $^{g}|1,+1\rangle$ magnetic sublevel is stronger than that from the $^{g}|1,-1\rangle$ sublevel. Attention should be paid to the fact that absorption from the lowest sublevel, with a spin projection $M_S = +1$, takes place for both right and left circularly polarised light. The C-term-related difference between the absorption coefficients for σ^{+}- and σ^{-}-polarised light is

$$\Delta A \sim N_{+1}\left|\langle 1,+1|^{g}m_{+}^{e}|2,0\rangle\right|^{2} + N_{-1}\left|\langle 1,-1|^{g}m_{+}^{e}|2,-2\rangle\right|^{2}$$
$$- N_{+1}\left|\langle 1,+1|^{g}m_{-}^{e}|2,+2\rangle\right|^{2} - N_{-1}\left|\langle 1,-1|^{g}m_{-}^{e}|2,0\rangle\right|^{2}, \quad (4)$$

where $N_{\pm1}$ are the populations of the corresponding levels; $m_{\pm} = \mp 1/\sqrt{2}\,(m_x \pm im_y)$ is a transition operator; and m_x and m_y are the projections of the transition operator onto the x and y axes. For simplicity, we introduce the notation

$$A_{10} = \left|\langle 1,\pm1|^{g}m_{\pm}^{e}|2,0\rangle\right|^{2},$$

$$A_{12} = \left|\langle 1,\pm1|^{g}m_{\mp}^{e}|2,\pm2\rangle\right|^{2}. \quad (5)$$

Figure 9. Schematic of the experimental setup.

Relation (4) then takes the following form:

$$\Delta A \sim N_{+1}A_{10} + N_{-1}A_{12} - N_{+1}A_{12} - N_{-1}A_{10}$$

$$= \Delta N(A_{10} - A_{12}), \tag{6}$$

where $\Delta N = N_{+1} - N_{-1}$ is the difference in population between the sublevels of the ground state spin doublet. Thus, the (paramagnetic) C-term of MCD can cause the absorption coefficients for σ^+- and σ^--polarised light to differ only if the two inequalities $\Delta N \neq 0$ and $A_{10} \neq A_{12}$ are satisfied. Solving rate equations for the system under consideration demonstrates that, even at identical A_{10} and A_{12}, the magnitude of the effect may reach $\sim 10^{-6}$ owing to the nonzero (diamagnetic) A-term. Measuring ΔA as a function of magnetic field at various temperatures, one can separately assess the contributions of the C- and A-terms.

Figure 9 shows a schematic of the experimental setup used to measure MCD via photoluminescence. The beam from a Ti:sapphire pump laser (Coherent Inc.), tuned to a wavelength $\lambda_{exc} = 1010$ nm, is further vertically polarised by a Glan prism. A photoelastic modulator (PEM), with its axis oriented at 45° to the plane of polarisation of the incident light, periodically switches the laser light between the σ^+- and σ^--polarisations. To reduce the contribution of the pump light to the measured luminescence intensity, an interference filter eliminating wavelengths shorter than 1086 nm (Semrock, BLP01-1064R-25) was placed in front of the monochromator. In addition, a depolariser was used to eliminate possible monochromator-induced polarisation effects. Figure 10 shows the NIR luminescence spectrum obtained under excitation at $\lambda_{exc} = 1010$ nm and $T = 1.6$ K. The spectrum does not have any features and is identical to the luminescence spectrum obtained under excitation at $\lambda_{exc} = 532$ nm (Fig. 2). Clearly, ΔI_{PL} can be directly measured in experiments. Figure 11 presents an example of a measured signal. It is seen that the total luminescence intensity is sinusoidally modulated at the frequency of the photoelastic modulator and that the σ^+ component of the pump light is absorbed more strongly than the σ^- component, which is consistent with the MCD sign measured around 500 nm. As follows from the above figures, the MCD signal is very weak. For example, at a temperature of 1.6 K in
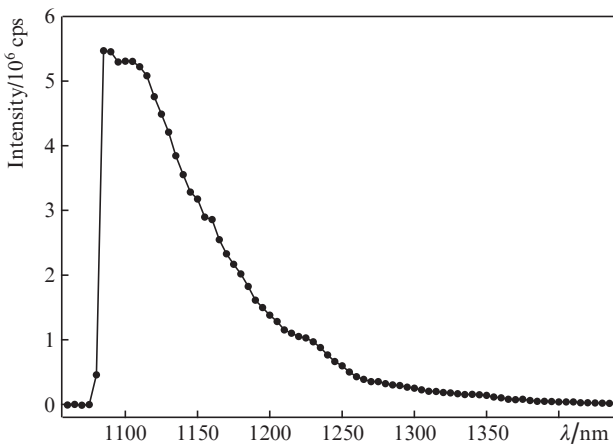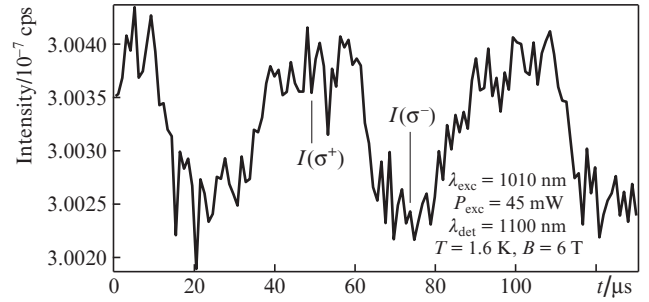
Figure 11. Time dependence of the total PL intensity at a wavelength $\lambda = 1100$ nm and periodically modulated pump polarisation.
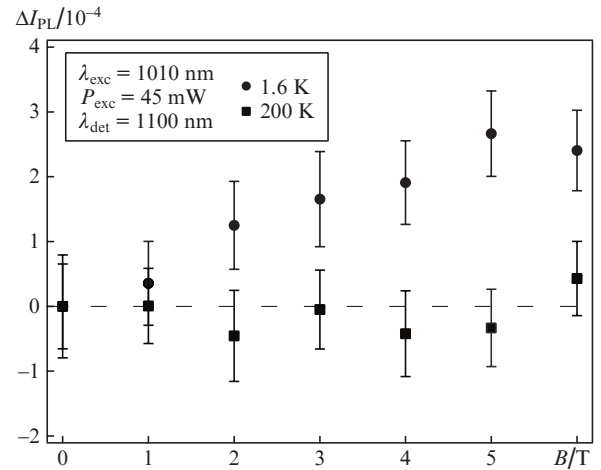
Figure 12. ΔI_{PL} as a function of magnetic induction at $T = 1.6$ and 200 K.

a magnetic field of 6 T, we have $\Delta I_{PL} = (2.4 \pm 0.6) \times 10^{-4}$ (Fig. 12). This indicates that the system corresponds to the last scheme considered by us, with a spin-triplet ground state and a quintet excited state.

To assess the exact nature of this signal, we measured ΔI_{PL} as a function of magnetic induction at various sample temperatures. Figure 12 presents the results for only two temperatures: 1.6 and 200 K. It is well seen that, at the low temperature, the signal rises with increasing magnetic induction. As mentioned above, all the components of the MCD signal (A, B and C) depend on the magnetic field. Nevertheless, at $T = 200$ K the signal amplitude oscillates around zero to within measurement accuracy. The complete disappearance of the effect is caused by the equalisation of the populations of the magnetic sublevels of the ground state. The experiment in question provides conclusive evidence that the ground state of the centre responsible for the NIR luminescence is a spin multiplet. Taking into consideration the excitation spectrum of the NIR luminescence band PL1, we arrive at the conclusion that, like the NIR luminescence, all the bands in the D series are due to the same centre. Moreover, we assume that the ground and first excited states of the centre are a spin triplet and spin quintet, respectively, because it is in this case that order-of-magnitude model estimates of ΔI_{PL} agree well with experimental data. However, any odd-electron systems and singlet ground state centres can be excluded with certainty. Thus, we are led to assume that the optical centre under discussion is a defect in the glass structure.


Figure 10. PL spectrum obtained under excitation at $\lambda_{exc} = 1010$ nm and $T = 1.6$ K. The wavy shape of the spectrum is caused by the transmission of the interference filter.

4. A model of luminescence centres

MCD experiments in combination with excitation spectra suggest the presence of two luminescence centres. One of them has a nondegenerate ground state, so we assume that it is the monovalent ion Bi$^+$. The other centre has a triplet ground state, and relaxation from its first excited state gives rise to the NIR emission band. We assume that this centre is a defect in the glass network, which results from doping with bismuth and subsequent reduction of the bismuth to a monovalent state. Previously, Razdobreev et al. [12] studied the luminescence kinetics of a band at $\lambda = 730$ nm (B1 band) in Bi/Ga-codoped silica glass, an analogue of the aluminosilicate glass under investigation. Their results demonstrate that the low-temperature decay of this band is very well fitted under the assumption that there is energy transfer to the acceptor (activator). Given this, we assume that a similar mechanism is operative in the bismuth-doped Al–Mg–Si oxide glass.

We began to construct a consistent model of optically active centres from a quantitative analysis of electronic states of the Bi$^+$ ion. We performed numerical calculations based on the theory of the crystal field splitting of p^{2,4} electronic configurations [25, 26]. The specifics of these configurations is such that, for any point group, except C1 and Ci, the crystal field potential can be represented in the form of a sum with two independent parameters: B_0^2 and B_2^2 [25]. These parameters represent the axial and rhombic distortions of the local environment of an ion. The energy of electronic states was evaluated by diagonalising the full energy matrix. The matrix was set up using the complete basis set of all 15 states of the p^{2,4} configuration in order to take into account the strong spin–orbit coupling, which can be comparable to the interaction with the crystal field.

Figure 13a presents the calculation results. Spin–orbit interaction splits the ground state term ^{3}P into three components: ^{3}P$_0$, ^{3}P$_1$ and ^{3}P$_2$. A crystal field of axial symmetry further splits them, producing two nondegenerate – A2 [^{3}P$_1$ ($M_J = 0$)] and A1 [^{3}P$_2$ ($M_J = 0$)] – and three doubly degenerate – E [^{3}P$_1$ ($M_J = \pm1$)], E [^{3}P$_2$ ($M_J = \pm1$)] and E [^{3}P$_2$ ($M_J = \pm2$)] – excited states. Following Griffith [26, 27], these states are denoted as 1Σ^-, 2Σ^+, 1Π, 2Π and 1Δ, respectively, and the ground state A1 (^{3}P$_0$) is denoted as 1Σ^+. Varying the Slater electron-repulsion integral F_2, the spin–orbit interaction constant Λ and the parameter B_0^2, we fitted the energy of these states to the positions of the corresponding bands in the B series, namely 14 285 ($\lambda = 700$ nm), 15 974 ($\lambda = 626$ nm) and 22 727 cm^{-1} ($\lambda = 441$ nm). The best fit, with a standard deviation under 1%, corresponds to $F_2 = 1135$ cm^{-1}, $\Lambda = 5312$ cm^{-1} and $B_0^2 = -26\,920$ cm^{-1}. It is worth noting that the values of F_2 and Λ approach those in a free Bi$^+$ ion (1175 and 5840 cm^{-1}, respectively). This indicates that, most likely, the bismuth ion occupies an interstitial site, without forming chemical bonds with its local environment. Our calculations demonstrate that the B1 band should be assigned to the transition from the ground state 1Σ^+ to the doubly degenerate excited state 1Π and that the B2 and B3 bands are due to the 1$\Sigma^+ \rightarrow$ 2Σ^+ and 1$\Sigma^+ \rightarrow$ 2Π transitions, respectively. As pointed out by Bartram et al. [26], the 1$\Sigma^+ \rightarrow$ 1Σ^- transition is strictly forbidden in local symmetry C$_{3v}$, where the 1Σ^- state is pure. Rhombic distortion causes mixing with other states, making this transition partially allowed. It seems likely that, for this reason, we were able to observe this transition in anti-Stokes luminescence of silica glass codoped with Ga and Bi [28]. Nevertheless, the transition remains very weak and is difficult to observe. Similar reasoning is applicable to the 1Σ^+ $\rightarrow$ 1Δ transition. In a local environment of C$_{3v}$ symmetry, the wave function of the E (1Δ) state consists predominantly (by
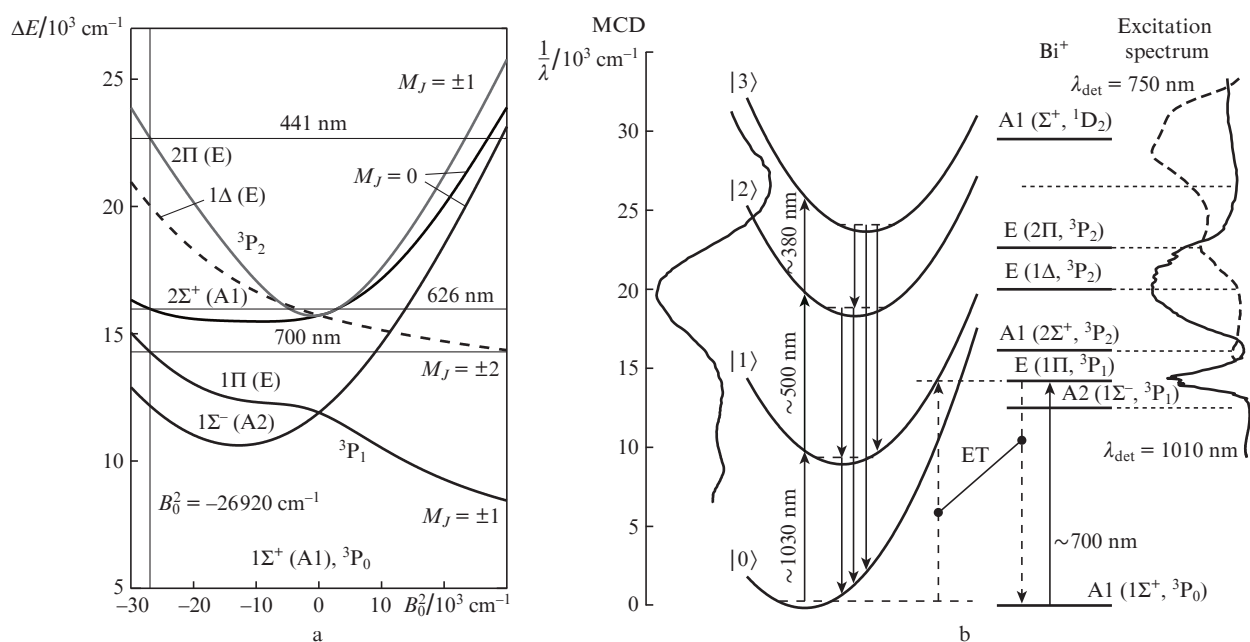
Figure 13. (a) Energy levels as functions of the axial parameter B_0^2 for the Bi$^+$ ion in a crystal field. The horizontal lines represent experimentally determined peak positions of the B1, B2 and B3 bands. (b) A model of interacting centres. Only one channel of energy transfer (ET) between the defect and Bi$^+$ ion is shown. Pumping at $\lambda = 500$ nm leads to excitation of the defect. Pumping at $\lambda = 700$ nm leads to direct excitation of the Bi$^+$ ion, which is accompanied by energy transfer to vibronic levels of the $|1\rangle$ state of the defect.

about 90%) of the $|112 \pm 2\rangle$ atomic state, with an admixture ($\sim$10%) of the $|022 \pm 2\rangle$ state [$^1D_2$ ($M_J = \pm 2$)]. Clearly, this transition is dipole-forbidden. Rhombic distortion, in turn, makes it weakly allowed. For this reason, it is also difficult to observe.

The axial parameter B_0^2 obtained here is rather large. The energy of the $^1D_2$ state evaluated in the proposed model exceeds 35 000 cm^{-1}, and the energy of the transition responsible for the B4 band is approximately 30 000 cm^{-1}. We think that, in the case of such a strong crystal field, the model is near its applicability limit, at least for high-energy states. Because of this, we assign the B4 band to the $^3P_0 \rightarrow {}^1D_2$ transition of the Bi$^+$ ion.

Figure 13b shows the energy-level diagram for defect–Bi$^+$ interaction and the corresponding excitation and MCD spectra. The diagram accounts for all the features observed in the spectra. Near-infrared luminescence is observed as a transition from the first excited state of the defect: $|1\rangle \rightarrow |0\rangle$. Owing to the energy transfer process, NIR luminescence can also be observed under excitation of the E (1Π) level of the bismuth ion at a wavelength of 700 nm. The absence of absorption bands in the NIR region and the long lifetimes indicate that the $|0\rangle \leftrightarrow |1\rangle$ transition is forbidden. Kalita et al. [29] observed a strong absorption from the $|1\rangle$ excited state at wavelengths under 1000 nm. We interpret this as evidence that the $|1\rangle \leftrightarrow |2\rangle$ transition is allowed. If this is so, under excitation to the $|2\rangle$ state the $|2\rangle \rightarrow |1\rangle$ transition should be rather fast and, moreover, it should show up in the spectrum as long-
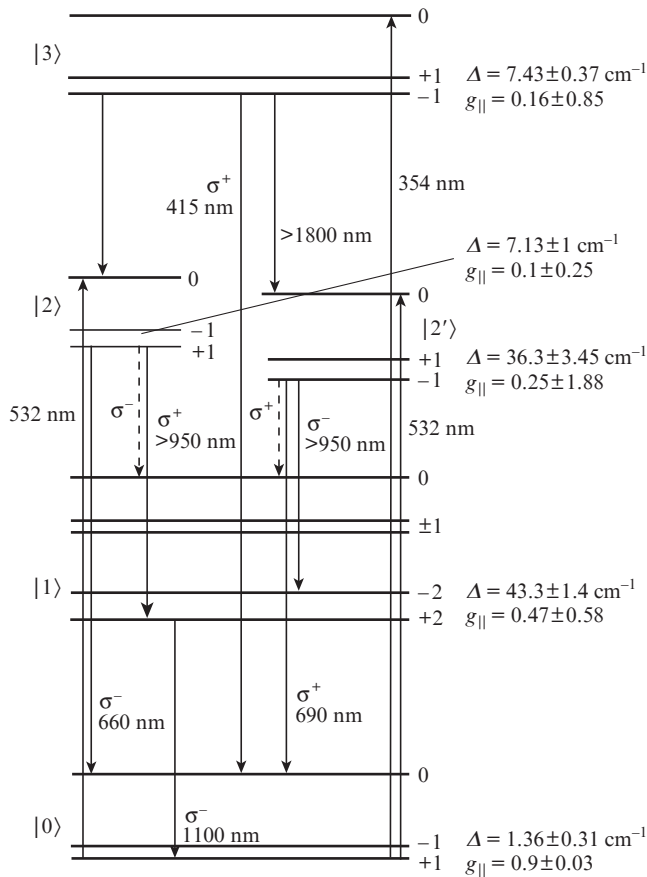
wavelength NIR luminescence with $\lambda \gtrsim 900$ nm. The red luminescence is in turn the result of the $|2\rangle \rightarrow |0\rangle$ allowed transition. It is easy to see that allowed luminescence wavelengths for this transition should lie in the range 550–950 nm.

As shown above, the effective spin of the $|0\rangle$ and $|1\rangle$ states of the defect in question is 1 and 2, respectively. Given this, the simplest energy-level diagram of the defect has the form presented in Fig. 14. This model successfully accounts for the unusual temperature dependences of the MCPL at detection wavelengths of 660 and 700 nm (Fig. 7). In this model, all the levels are spin triplets, except for the first excited state $|1\rangle$, whose effective spin is $S = 2$. Pumping at $\lambda_{exc} = 532$ nm excites two closely spaced states: $|2\rangle$ and $|2'\rangle$. In the MCD and absorption spectra, the $|0\rangle \rightarrow |2\rangle$ and $|0\rangle \rightarrow |2'\rangle$ transitions show up as the D2 band, which peaks near $\lambda = 500$ nm. The two MCPL bands opposite in sign, peaking at $\lambda = 660$ and 690 nm, are due to transitions from the lower spin sublevels with $M_S = +1$ and $M_S = -1$ of the $|2\rangle$ and $|2'\rangle$ states to the ground state $|0\rangle$, respectively. As a result of the selection rules for the MCPL ($\Delta M_S = -1$ for σ$^-$-polarised light and $\Delta M_S = +1$ for σ$^+$-polarised light), the transition from the $M_S = +1$ sublevel of the $|2\rangle$ state to the $M_S = 0$ sublevel of the ground state ($\lambda = 660$ nm) is responsible for the negative component of the MCPL signal. The positive MCPL component corresponds to the $|2'\rangle$ ($M_S = -1$) $\rightarrow |0\rangle$ ($M_S = 0$) transition. Pumping at a wavelength $\lambda_{exc} = 354$ nm leads to the excitation to the $|3\rangle$ state. Subsequent relaxation can follow three channels. One channel is the $|3\rangle \rightarrow |0\rangle$ transition, which shows up as the MCPL and PL bands near $\lambda = 430$ nm (Fig. 4). Another channel, $|3\rangle \rightarrow |2(2')\rangle$, should show up in the NIR region at wavelengths above 1800 nm and, to the best of our knowledge, has not yet been detected. As a result of spin–lattice relaxation, the lower sublevels of the $|2\rangle$ and $|2'\rangle$ states become populated, which leads to the presence of two components of the MCPL signal near $\lambda = 700$ nm, as discussed above. The third channel is the $|3\rangle \rightarrow |1\rangle$ transition and

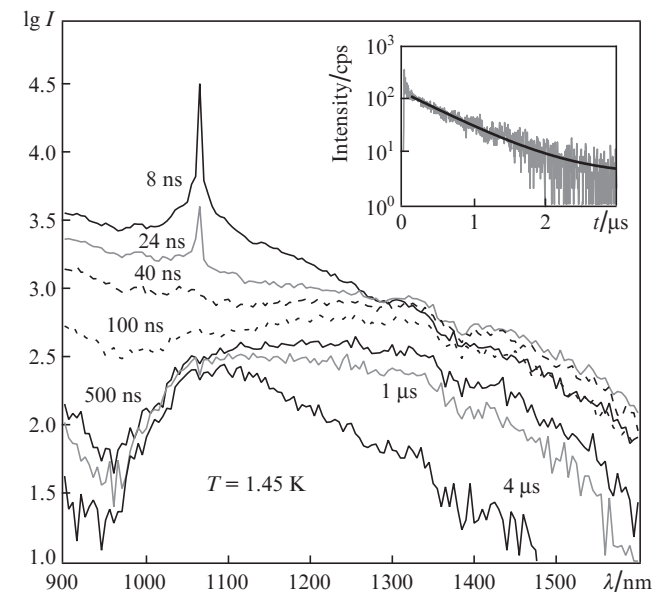**Figure 14.** Energy-level diagram of the defect.

Figure 15. NIR luminescence spectra at various time delays relative to the excitation pulse. Inset: luminescence decay kinetics at a wavelength of 1550 nm.

should have an intensity peak near $\lambda = 650$ nm. In our model, emission from the lower sublevel ($M_S = -1$) of the $|3\rangle$ state has σ^+- and σ^--polarised components comparable in intensity. Therefore, the total degree of luminescence polarisation should be near zero.

In addition, the model explains the characteristic features of the NIR luminescence decay kinetics. As shown by Denker et al. [10], the NIR luminescence decay in bismuth-doped aluminosilicate glass has a slow ($\tau \approx 800$ µs) and a fast ($\tau \approx 2$ µs) components. Similar behaviour was observed in Ga/Bi-codoped silica glass [12]. According to our model, the near-infrared PL should comprise two components, corresponding to the $|1\rangle \rightarrow |0\rangle$ and $|2(2')\rangle \rightarrow |1\rangle$ transitions. To confirm this hypothesis, we obtained time-resolved NIR luminescence spectra (Fig. 15) under excitation with subnanosecond pulses ($\Delta t = 400$ ps) at a wavelength of 532 nm. In the initial stage, there is a strong luminescence peak near $\lambda = 1060$ nm, due to the fluorescence line narrowing. The luminescence decay time is ~ 4 µs over the entire spectral range studied. The boundary wavelengths of the $|1\rangle \rightarrow |0\rangle$ forbidden transition are approximately 950 and 1500 nm. To accurately determine the fast luminescence lifetime, measurements were made at a wavelength of 1550 nm. The inset in Fig. 15 illustrates the luminescence decay kinetics at this wavelength. The luminescence decay is well represented by a single exponential, with a lifetime $\tau \approx 0.64 \pm 0.01$ µs. Thus, the above assumption that the $|2(2')\rangle \rightarrow |1\rangle$ fast transition can be observed is confirmed experimentally.

Point defects and localised states formed by the Bi 6p, Pb 6p, Sn 5p and Sb 5p states were first proposed as possible NIR luminescence sources by Sharonov et al. [30, 31]. They did not propose any particular microscopic model of an emission centre but concluded that the major absorption and emission peaks were not necessarily due to the same centre. In a model recently proposed by Dianov [32], a Bi^{2+} ion and oxygen vacancy [ODC(II) centre] form a single luminescence centre (or a molecule). In that model, the optically active centre has the form of an odd-electron system with a total angular momentum $J = 1/2$ in its ground state. Clearly, that model is inconsistent with our experimental data. For the same reasons, Bi^{5+} [2] and Bi^{2+} ions, BiO molecules [33], Bi^0 atoms [34] and Bi^{2-} dimers [35] should be excluded from the list of possible candidates.

5. Conclusions

Bismuth-doped Mg–Al–Si oxide glass has been studied in detail by MCD and MCPL spectroscopies. Using conventional laser spectroscopies as well, we have demonstrated the coexistence of at least three distinct optical centres. Analysis of MCD and MCPL signals as functions of magnetic field and temperature has shown that all three centres have an even number of electrons or holes. Two of them have a degenerate ground state and are responsible for the MCD signal. We assume that the Ci MCD bands in the near-IR region are due to bismuth ion clusters. The other two centres are identified as the Bi^+ ion and, tentatively, as a defect in the glass structure. There is energy transfer between these centres, but they do not form a single molecule or a single luminescence centre. The proposed model of optical centres successfully accounts for all characteristic features of the present experimental data. In this model, the NIR luminescence is due to a forbidden transition from the first excited state of the defect. Owing to

energy transfer, this NIR luminescence can also be observed under excitation to the E ($^3P_1$, $M_J = \pm 1$) state of the Bi^+ ion ($\lambda_{exc} = 700$ nm). It is shown that the red luminescence is also due to the intracentre transition from the second excited state of the defect to its ground state.

References

1. Murata K., Fujimoto Y., Kanabe T., Fujita H., Nakatsuka M. *Fusion Eng. Des.*, **44**, 437 (1999).
2. Fujimoto Y., Nakatsuka M. *Jpn. J. Appl. Phys.*, **40**, L279 (2001).
3. Dianov E.M. *Light: Sci. Appl.*, **1**, 1 (2012).
4. Duarte F.J. (Ed.). *Tunable Laser Applications* (New York: CRC, 2016).
5. Peng M., Dong G., Wondraczek L., Zhang L., Zhang N., Qiu J. *J. Non-Cryst. Solids*, **357**, 2241 (2011).
6. Stephens P.J. *Annu. Rev. Phys. Chem.*, **25**, 201 (1974).
7. Riehl J.P., Richardson F.S. *J. Chem. Phys.*, **65**, 1011 (1976).
8. Laguta O., El Hamzaoui H., Bouazaoui M., Arion V.B., Razdobreev I. *Optica*, **2**, 663 (2015).
9. Serber R. *Phys. Rev.*, **41**, 489 (1932).
10. Denker B., Galagan B., Osiko V., Shulman I., Sverchkov S., Dianov E. *Appl. Phys. B*, **95**, 801 (2009).
11. Denning R.G., in *Electronic States of Inorganic Compounds: New Experimental Techniques: Lectures Presented at the NATO Advanced Study Institute held at the Inorganic Chemistry Laboratory and St. John's College*. Ed. by P. Day (Dordrecht: Springer, 1975) pp 157–176.
12. Razdobreev I., El Hamzaoui H., Arion V.B., Bouazaoui M. *Opt. Express*, **22**, 5659 (2014).
13. Meng X., Qiu J., Peng M., Chen D., Zhao Q., Jiang X., Zhu C. *Opt. Express*, **13**, 1635 (2005).
14. Zhou S., Jiang N., Zhu B., Yang H., Ye. S., Laksshminaranayana G., Hao J., Qiu J. *Adv. Funct. Mater.*, **18**, 1407 (2008).
15. Mason W.R. *A Practical Guide to Magnetic Circular Dichroism Spectroscopy* (New York: Wiley, 2007).
16. Laguta O., Denker B., Galagan B., Sverchkov S., Razdobreev I. *Opt. Quantum Electron.*, **48**, 123 (2016).
17. Solomon E.I., Pavel E.G., Loeb K.E., Campochiaro C. *Coord. Chem. Rev.*, **144**, 369 (1995).
18. Abragam A., Bleany B. *Electron Paramagnetic Resonance of Transition Ions* (London: Oxford University Press, 1970).
19. Schatz P.N., Mowery R.L., Krausz E.R. *Mol. Phys.*, **35**, 1537 (1978).
20. Weil J., Bolton J. *Electron Paramagnetic Resonance: Elementary Theory and Practical Applications* (Hoboken: John Wiley & Sons, 2007).
21. Ren J., Dong G., Xu S., Bao R., Qiu J. *J. Phys. Chem.*, **112**, 3036 (2008).
22. Ruan J., Su L., Qiu J., Chen D., Xu J. *Opt. Express*, **17**, 5163 (2009).
23. Peng M., Sprenger B., Schmidt M.A., Schwefel H.G.L., Wondraczek L. *Opt. Express*, **18**, 12852 (2010).
24. Skuja L. *J. Non-Cryst. Solids*, **239**, 16 (1998).
25. Davis H.L., Bjerrum N.J., Smith G.P. *Inorg. Chem.*, **6**, 1172 (1967).
26. Bartram R.H., Fockele M., Lohse F., Spaeth J.-M. *J. Phys.: Condens. Matter*, **1**, 27 (1989).
27. Griffith J.S. *The Theory of Transition-Metal Ions* (Cambridge: Cambridge Univ. Press, 2009) p. 455.
28. Laguta O., El Hamzaoui H., Bouazaoui M., Arion V.B., Razdobreev I. *Opt. Lett.*, **40**, 1591 (2015).
29. Kalita M.P., Yoo S., Sahu J. *Opt. Express*, **16**, 21032 (2008).
30. Sharonov M.Y., Bykov A.B., Petricevic V., Alfano R.R. *Opt. Lett.*, **33**, 2131 (2008).

31. Sharonov M.Y., Bykov A.B., Alfano R.R. *J. Opt. Soc. Am. B*, **26**, 1435 (2009).
32. Dianov E.M. *Laser Phys. Lett.*, **12**, 095106 (2015).
33. Ren J., Yang L., Qiu J., Chen D., Jiang X., Zhu C. *Solid State Commun.*, **140**, 38 (2006).
34. Peng M., Zollfrank C., Wondraczek L. *J. Phys.: Condens. Matter*, **21**, 285106 (2009).
35. Sokolov V.O., Plotnichenko V.G., Dianov E.M. *Opt. Lett.*, **33**, 1488 (2008).